Physica A 389 (2010) 1178–1188

Contents lists available at ScienceDirect

Physica A

journal homepage: www.elsevier.com/locate/physa

Effects of surface size on minimalistic stochastic models for the catalytic CO oxidation

M. Pineda [a,*], R. Imbihl [b], L. Schimansky-Geier [c]

[a] IFISC Instituto de Física Interdisciplinar y Sistemas Complejos (CSIC-UIB), E-07122 Palma de Mallorca, Spain
[b] Institut für Physikalische Chemie und Elektrochemie, Leibniz Universität Hannover, Callinstraße 3-3a, D-30167 Hannover, Germany
[c] Institut für Physik, Humboldt Universität zu Berlin, Newton Straße 15, D-12489 Berlin, Germany

ARTICLE INFO

Article history:
Received 21 August 2009
Available online 20 November 2009

Keywords:
CO oxidation
Monte Carlo simulations
Master equation

ABSTRACT

The impact of surface size on two minimalistic models for the bistable CO oxidation is analytically studied. A simple model for the catalytic CO oxidation on nanoscale surfaces is analyzed by the chemical master equation. The analytical results predict a shift of the bistable region and cusp point in the global bifurcation diagram as a function of surface size. A reaction–diffusion stochastic model consisting of a collection of reactive subdomains locally coupled by CO diffusion is also considered. A local description of fluctuations can be obtained after applying a Weiss-type mean-field approximation. This approximation predicts, for infinitely many subdomains, a break of ergodicity and a bifurcation behavior like in first-order phase transitions as a function of surface size and coupling parameter. Analytical results are compared with Gillespie-type Monte Carlo simulations.

1. Introduction

One of the most important problems in nonlinear surface reactions on the nanometer scale are so-called size effects, i.e., the dependence of the global reaction kinetics on the size of the active surfaces. Examples of such nanoscale kinetic phenomena are the communication effects resulting from the coupling of surface areas with different reaction behavior through surface diffusion [1,2] or coverage fluctuations in very small surfaces [3–6]. As the relative amplitude of fluctuations in a system scales with $N^{-1/2}$ (N being the number of molecules involved), an important influence is expected on the length scale of a few nanometers. In this article, we present a theoretical analysis of the impact of surface size on minimalistic stochastic models for the bistable catalytic CO oxidation on small surfaces.

From a macroscopic point of view nonlinear surface reactions are usually modeled using reaction–diffusion rate equations, but from a microscopic point of view the reactive and nonreactive collision events must be taken into account. When the nonreactive or diffusive events are sufficiently frequent to remove any spatial inhomogeneities and the system is small enough, a homogeneous system with homogeneous coverage fluctuations is generated. Consequently, it can be described by stochastic mean-field models. Such situations can arise in CO oxidation on a field emitter tip where coverage fluctuations on different nanofacets are largely uncorrelated, while a high degree of spatial correlations exist only for fluctuations on a single facet [3–5]. This means that a single nanofacet can be approximated as well-stirred homogeneous system allowing nonlinear behavior and homogeneous coverage fluctuations [7–9]. The CO oxidation on nanofacets of Pd nanoparticles represents another example of a well-stirred homogeneous system and a stochastic approach with mean-field models was used to clarify recent experimental findings [6]. Mean-field stochastic models have been also used to predict an optimal particle size for reaction rate oscillations in CO oxidation on nanometer-sized palladium particles and NO reduction by CO on platinum surfaces [10,11].

* Corresponding author. Tel.: +32 2 6505798; fax: +32 2 6505767.
E-mail address: mpineda@ulb.ac.be (M. Pineda).

0378-4371/$ – see front matter © 2009 Elsevier B.V. All rights reserved.
doi:10.1016/j.physa.2009.11.024

On the other hand, if the diffusion is weak enough or if the system is large enough, the spatial homogeneity will be destroyed and local fluctuations begin to play an important role. In this case, spatially extended stochastic models are needed [12,13]. This situation can also be found in CO oxidation on a field emitter tip when the coupling between nanofacets through CO diffusion is taken into account. It is known that CO diffusion is very fast within a facet but partially inhibited by structural heterogeneities at the periphery of the facet, e.g., due to strongly reduced CO diffusion across steps or an enhanced reactivity at step sites. Under these circumstances, the reaction behavior occurs on a set of coupled nanofacets [1]. Diffusion of adsorbed particles can also be reduced at high pressure. By increasing the pressure, the number of gas particles impinging on the surfaces grows and, therefore, the surface residence time decreases. Simultaneously, the total adsorbate coverage will approach the saturation limit and, since surface diffusion requires vacant sites, the diffusion rate will become very low. Finally, the combined effect will lead to a smaller and smaller diffusion length with rising pressure and to the formation of very small well-stirred subregions coupled by diffusion. Stochastic patterns (''raindrop patterns'') observed in catalytic CO oxidation at high pressure were interpreted in this way [14,15].

In this work, we analyze the impact of surface size on two minimalistic models for the catalytic CO oxidation on small surfaces. For that purpose, we consider a stochastic mean-field model that mimics the behavior of the bistable CO oxidation on a single uncoupled nanofacet. We show analytically a shift of bistable regions and of cusp bifurcation points as a function of surface size. Theoretical results are compared with simulations using the direct Gillespie algorithm [16]. We also consider a spatially extended stochastic model to analyze the behavior of the bistable CO oxidation under reduced mobility of CO molecules. We consider a square lattice of subdomains locally coupled by CO diffusion. Each such subdomain may contain far fewer particles than the entire system and may behave like a well-stirred homogeneous region allowing bistability and homogeneous coverage fluctuations. We use a Weiss-type mean-field approximation as a first mathematical treatment to analyze local fluctuations. This approximation predicts a first-order phase transition connected with a breaking of ergodicity in an array of globally coupled subdomains depending on surface size and coupling parameter. Although in this approximation local diffusion exchange is replaced by a global (all to all) coupling, the Weiss mean-field results provide a better understanding of our two dimensional spatially extended model with local coupling. The theoretical results are compared with stochastic simulations based on an extended version of Gillespie algorithm, which has been inspired by the next subvolume method introduced by Elf and Ehrenberg [16,17].

This article is organized as follows. The bifurcation behavior of our stochastic mean-field model for CO oxidation on homogeneous small surfaces is analyzed in Section 2. Section 3 is devoted to study the impact of surface size and CO diffusion in a spatially extended stochastic model for CO oxidation under reduced CO mobility. Summary and conclusions are presented in Section 4.

2. CO oxidation on small surfaces: Finite-size shift in bistable regions

As a consequence of high CO mobility, the catalytic CO oxidation on nanoscale surfaces can be considered as a well-stirred system. On a nanoscale, given the small surface area, size effects also become important and this is the motivation to study in this section a minimalistic stochastic mean-field model for the bistable CO oxidation on nanoscale surfaces (i.e. a single nanofacet of a Pt field emitter tip or nanoparticle). We will show analytically and by simulations that the macroscopic bifurcation behavior of the bistable CO oxidation is affected by the surface size.

The elementary steps of CO oxidation on noble metal surfaces such as Pt, Pd, and Ir are determined by Langmuir–Hinshelwood (LH) mechanism which consists of the steps

$$\begin{aligned}
&\mathrm{CO(gas)} + * \longleftrightarrow \mathrm{CO(ads)},\\
&\mathrm{O_2(gas)} + 2* \longrightarrow 2\mathrm{O(ads)},\\
&\mathrm{CO(ads)} + \mathrm{O(ads)} \longrightarrow \mathrm{CO_2(gas)} + 2*,
\end{aligned}$$

with $*$ and (ads) denoting a vacant adsorption site and adsorbed molecules or adatoms, respectively. On a macroscopic large surface, bistability is considered to be the most prominent feature of the reaction presented above. In this bistable state, two kinetic stationary states coexist. The active steady state, where the surface is predominantly oxygen covered, and the inactive steady state, where a high CO coverage inhibits O_2 adsorption and hence poison the reaction. Depending on the initial conditions, the system resides on one of the two stationary stable states for an indefinite period of time. This phenomena can be described very well with ordinary differential equations [18]. However, it is well known that the macroscopic description breaks down when the surface area is of nanoscale dimensions [8,19]. For instance, with decreasing surface area reaction-induced coverage or molecular fluctuations become important and transitions between the two stable states start to occur [3,8,6].

In order to study correctly size effects and bistability in CO oxidation on very small surfaces, the starting point is to define the transition rates and population changes of the particle number of carbon monoxide (N_{CO}) and oxygen (N_{O}) caused by reactive events described above. Since we are assuming a well-mixed system, the transition probabilities are given by the mass-action law according to

$$W_1(N_{\mathrm{CO}}/N_{\mathrm{CO}}+1) = Ap_{\mathrm{CO}}\left[1-\left(\frac{N_{\mathrm{CO}}}{A}\right)^2\right], \tag{1}$$

$$W_2(N_{CO}/N_{CO}-1) = dN_{CO}, \tag{2}$$

$$W_3(N_O/N_O+2) = \frac{p_{O_2}}{A}(A-N_{CO}-N_O)(A-N_{CO}-N_O-1), \tag{3}$$

$$W_4(N_{CO},N_O/N_{CO}-1,N_O-1) = \frac{4kN_ON_{CO}}{A}, \tag{4}$$

where $W_1(N_{CO}/N_{CO}+1)$ represents the transition probability per unit time to increase the number of CO molecules from N_{CO} to $N_{CO}+1$. The same interpretation is given to the other transition probabilities. Note that $0 < N_{CO}+N_O \leq A$, where the parameter A represents the area of the small reacting surface and, therefore, it determines the intensity of the fluctuations. The parameters p_{CO} and d are, respectively, the CO(gas) adsorption and CO(ad) desorption rates. The exponent 2 models the precursor-type kinetics of CO adsorption [18]. We consider that while preadsorbed CO inhibits dissociative adsorption of oxygen, no such siteblocking effect is exerted by oxygen on incoming CO molecules. The dissociatively O_2(gas) adsorption rate and the CO and oxygen reaction rate are set $p_{O_2} = 0.25$ and $k = 100$, respectively. At the end, three parameters, p_{CO}, d, and A are left for variation.

The stochastic behavior of the system is described by the probability distribution function $P(\mathbf{Z};t)$ of finding a set of populations $\mathbf{Z} = \{N_{CO}, N_O\}$. This probability distribution is governed by the well-known master equation which results from the transition probabilities W_σ, where σ runs from 1 to 4. This master equation is written as

$$\frac{d}{dt}P(\mathbf{Z};t) = \sum_{\rho=1}^{4}[W_\rho(\mathbf{Z}-\mathbf{v}_\rho/\mathbf{Z})P(\mathbf{Z}-\mathbf{v}_\rho;t) - W_\rho(\mathbf{Z}/\mathbf{Z}-\mathbf{v}_\rho)P(\mathbf{Z};t)]. \tag{5}$$

This equation is essentially a stochastic mean-field description. Instead of microscopic configurations and processes of adsorbates, one tracks only the total numbers or coverages of adsorbates of different species and their increment and decrement. In most cases, it is difficult or impossible to solve this equation. However, several approximation techniques have been proposed. In this work, we use the so-called adiabatic or quasi-steady state approximation, where one considers a time-scale separation, where a subset of species is asymptotically at steady state on the long-time scale [8,20]. Remarkably, it has been already shown that for CO oxidation on surfaces this kind of time-scale separation exits [8,21]. In particular, one can show that the fast oxygen variable goes towards a partial equilibrium conditioned by the slow CO variable. Therefore, our first challenge is to eliminate adiabatically the fast oxygen variable N_O from the master equation (5).

To carry out this elimination, we decompose the joint probability as

$$P(\mathbf{Z};t) = G(N_{CO};t)g(N_O|N_{CO};t), \tag{6}$$

where $g(N_O|N_{CO};t)$ is the conditional probability for N_{CO} kept constant and $G(N_{CO};t)$ is the probability distribution function for the occupation of the surface with N_{CO} molecules [8]. We also require $\sum_{N_{CO}} G(N_{CO}) = 1$ and $\sum_{N_O} g(N_O|N_{CO}) = 1$. Inserting Eq. (6) into the master equation (5) and summing up over N_O, we obtain after several approximations [8]

$$\frac{dG(N_{CO};t)}{dt} = H_1(N_{CO}-1)G(N_{CO}-1;t) - H_1(N_{CO})G(N_{CO};t) + H_2(N_{CO}+1)G(N_{CO}+1;t) - H_2(N_{CO})G(N_{CO};t), \tag{7}$$

where the new transition probabilities are:

$$H_1(N_{CO}/N_{CO}+1) = Ap_{CO}\left[1-\left(\frac{N_{CO}}{A}\right)^2\right], \tag{8}$$

$$H_2(N_{CO}/N_{CO}-1) = dN_{CO} + \frac{4k\langle N_O\rangle N_{CO}}{A}, \tag{9}$$

with $\langle N_O\rangle = \tilde{N}_O = \sum_{N_O} N_O g(N_O|N_{CO})$. Fortunately, there are several ways to obtain this first moment [8,22]. Since the time-scale separation between the two random variables N_O and N_{CO} is large enough, it can be shown that $g(N_O|N_{CO})$ is a sharply peaked unimodal function [8]. Therefore, the first moment can be approximated by the maxima of $g(N_O|N_{CO})$ which is given by $\tilde{N}_O = A\tilde{\theta}_O$, with the coverage $\tilde{\theta}_O$ obtained from Ref. [7]

$$\frac{d\tilde{\theta}_O}{dt} = \lim_{A\to\infty}\frac{2\langle W_3\rangle - \langle W_4\rangle}{A} \approx 0, \tag{10}$$

or more explicitly

$$2p_{O_2}(1-\theta_{CO}-\tilde{\theta}_O)^2 - 4k\theta_{CO}\tilde{\theta}_O \approx 0, \tag{11}$$

with $\theta_{CO} = N_{CO}/A$ being kept constant. This approximation holds true for small fluctuations in the fast variable. Now, it is straightforward to solve Eq. (11) to obtain

$$\tilde{\theta}_O = \left[1+\theta_{CO}\left(\frac{\gamma}{2}-1\right)\right] - \sqrt{\theta_{CO}\gamma\left[1+\theta_{CO}\left(\frac{\gamma}{4}-1\right)\right]}, \tag{12}$$

with $\gamma = 2k/p_{O_2}$. To find analytical results, we expand the square root in Eq. (12) into Taylor series to obtain (for $\theta_{CO} \neq 0$)

$$\tilde{\theta}_O \approx \frac{(\theta_{CO}-1)^2}{\gamma\theta_{CO}} + \frac{2(\theta_{CO}-1)^3}{\gamma^2\theta_{CO}^2}. \tag{13}$$

Then, we suppose that $G(N_{CO}; t)$ approaches a stationary shape including macroscopic transitions between the stable states of the deterministic approach. The final shape of $G(N_{CO}; t)$ should agree with the solution $dG^{st}(N_{CO})/dt = 0$, with boundary condition $G^{st}(N_{CO} \longrightarrow \infty) = 0$. In this case, detailed balance holds and one finds

$$G^{st}(N_{CO}) = \prod_{N=1}^{N_{CO}} \frac{H_1(N-1)}{H_2(N)} \left(1 + \sum_{n=1}^{A}\prod_{N=1}^{n} \frac{H_1(N-1)}{H_2(N)}\right)^{-1}. \tag{14}$$

This result allows us to introduce an analytical expression for the effective potential given by

$$\phi(N_{CO}) = \frac{-\ln G^{st}(N_{CO})}{A}, \tag{15}$$

which is useful to analyze the system size dependence of fluctuations [7].

Now, in order to characterize the number of maxima of $G^{st}(N_{CO})$ as a function of surface area A we have to find the parameters where

$$G^{st}(N_{CO}-1) = G^{st}(N_{CO}), \tag{16}$$

and taking into account detail balance we get

$$H_1(N_{CO}-1) = H_2(N_{CO}), \tag{17}$$

or more explicitly

$$\frac{F}{N_{CO}} = 0, \tag{18}$$

where

$$F = aN_{CO}^3 + bN_{CO}^2 + cN_{CO} + e, \tag{19}$$

and

$$a = \frac{4k}{A}\left(\frac{1}{\gamma} + \frac{2}{\gamma^2}\right) + \frac{p_{CO}}{A}, \tag{20}$$

$$b = -4k\left(\frac{2}{\gamma} + \frac{6}{\gamma^2}\right) + d - \frac{2p_{CO}}{A}, \tag{21}$$

$$c = 4kA\left(\frac{1}{\gamma} + \frac{6}{\gamma^2}\right) - Ap_{CO} + \frac{p_{CO}}{A}, \tag{22}$$

$$e = \frac{-8kA^2}{\gamma^2}. \tag{23}$$

To find the region of bistability, we consider at steady state the well-known condition [23]

$$\kappa = q^3 + r^2 < 0, \tag{24}$$

with

$$q = \frac{3ac - b^2}{9a^2}, \tag{25}$$

and

$$r = \frac{9abc - 27a^2e - 2b^3}{54a^3}. \tag{26}$$

Fig. 1 shows the bifurcation diagram in the parameter space (p_{CO}, d) for two values of A. This bifurcation diagram shows the bistable region for $A = 20$ (gray region) and 1000 (black region). It is clear that the theory predicts a shift of the bistable region with decreasing or increasing the surface area A. The bistable regions vanish as $d \to d_c(A)$, where $d_c(A)$ corresponds to a cusp bifurcation point (full big circles). The shift of this cusp bifurcation point is also evident [see inset of Fig. 1].

In order to get more insight into this effect, we study the solutions of $F = 0$ [Eq. (19)] which approximately represent stable and unstable extrema of $G^{st}(N_{CO})$. Note that due to the discrete character of our problem the real solutions of $F = 0$ are not identical with the extrema of $G^{st}(N_{CO})$, but they differ less than 1 from the extrema. Fig. 2 shows F for $p_{CO} = 0.39$

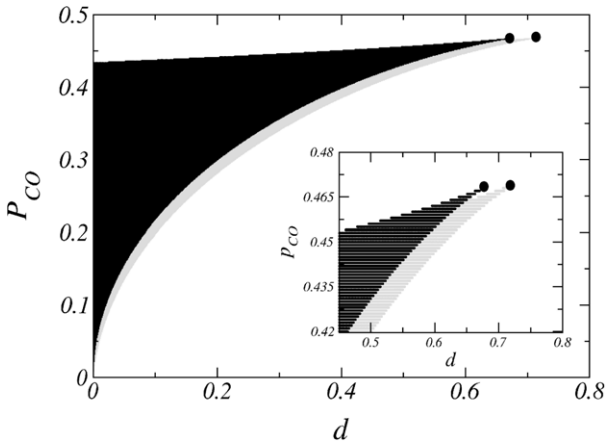

Fig. 1. Bifurcation diagram in the parameter space (p_{CO}, d) for $A = 20$ (gray) and $A = 1000$ (black). Inset shows a zoom around the cusp bifurcation point. The comparison of the two regions shows that a shift of the global bifurcation diagram is induced by changing the surface area A. We have fixed $p_{O_2} = 0.25$ and $k = 100$. Full big circles represent critical or cusp bifurcation points.

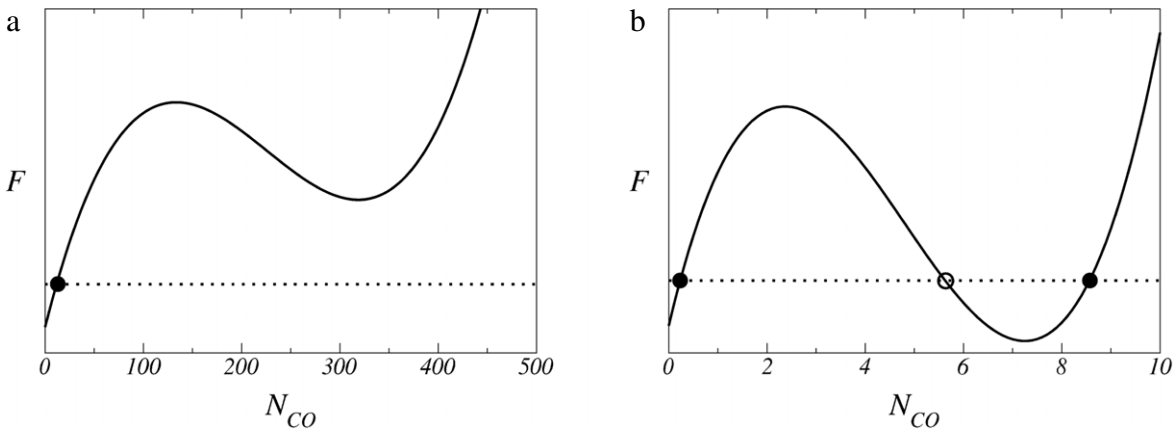

Fig. 2. Finite surface size induced bistability. Solutions of $F = 0$ represent stable and unstable maxima of $G^{st}(N_{CO})$. (a) For $A = 1000$, only one solution is obtained (solid dot). (b) For $A = 20$ three solutions appear, the two extreme solutions are stable (solid dots) and the intermediate one unstable (open dot). We have fixed $p_{CO} = 0.39$, $d = 0.4$, $p_{O_2} = 0.25$, and $k = 100$.

and $d = 0.4$. In Fig. 2(a), we plot F for $A = 1000$, and as expected from Fig. 1, only one stable solution exist (solid dot). However, Fig. 2(b) shows that for $A = 20$ three solutions exist for same parameter values. The two extreme solutions are stable (solid dots) and the intermediate one unstable (open dot). To the best of our knowledge, this is the first analytical study of a bistable surface reaction, revealing a shift of the bistable region with decreasing or increasing the surface area: Bistability changes into monostability and vice versa.

We have compared those theoretical results with stochastic simulations using the direct Gillespie algorithm [16]. Simulations for the original unreduced system are obtained from transition probabilities given by Eqs. (1)–(4). We have also shown simulations of the adiabatically reduced model with transition probabilities given by Eqs. (8) and (9) together with Eq. (12) to describe the behavior of the removed oxygen variable for $\theta_{CO} = N_{CO}/A$ fixed. Fig. 3 shows the probability distribution functions and effective potentials corresponding to Fig. 2. Theoretical results and simulations are presented by lines and symbols, respectively. As expected, simulation with the adiabatically reduced model (circles) reproduces very well the analytical results (solid lines). But, there are minor discrepancies with simulations coming from the original unreduced system (squares).

3. Compartmentalized surface reaction system: A local description of fluctuations

In Section 2, we have studied the impact of small isolated surfaces or nanofacets containing hundreds to thousand reacting particles on the bifurcation behavior of the bistable CO oxidation. What has been neglected in this study is the coupling between adjacent nanofacets. Experimentally, there is some justification for this, since one observes essentially no correlations between fluctuations on adjacent nanofacets of a Pt field emitter tip [5]. However, due to CO diffusion which is only reduced by atomic steps but not equal to zero some coupling between facets has to exist and, hence, there must be

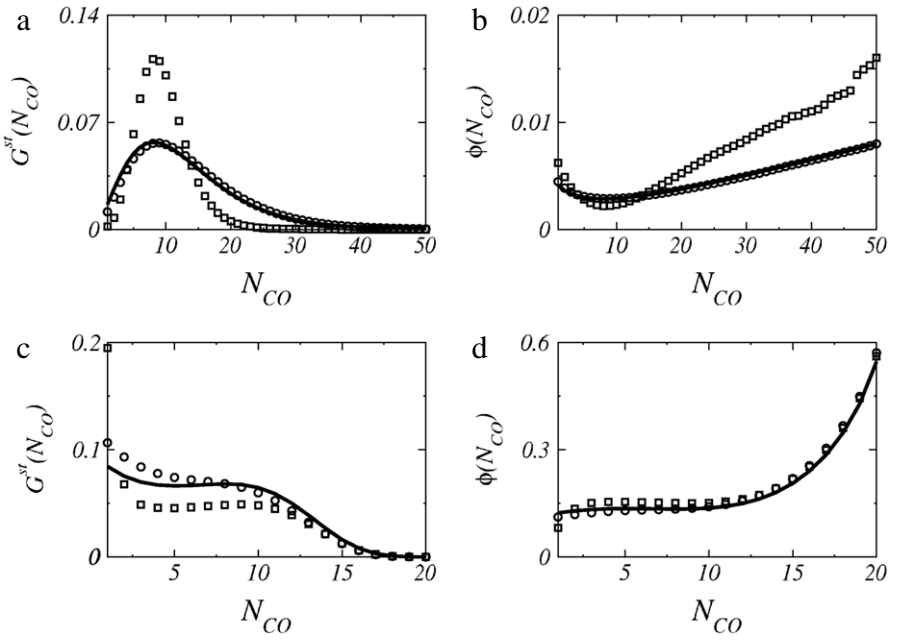

Fig. 3. Probability distributions and effective potentials for cases shown in Fig. 2. Top panels show the theoretical probability distribution function $G^{st}(N_{CO})$ and effective potential $\phi(N_{CO})$ for $A = 1000$ (solid lines). Note the mono-modality of those functions. In the botton panels, we show the theoretical probability distribution function $G^{st}(N_{CO})$ and effective potential $\phi(N_{CO})$ for $A = 20$ (solid lines). In this case, the probability distribution function is bimodal and the effective potential has a double-well structure representing a bistable behavior. Simulations are obtained using the direct Gillespie algorithm. Circles represent simulations from the adiabatically reduced model. Squares represent simulations from the original unreduced model.

some correlations between the fluctuations [1,2]. It has also been claimed that local coverage fluctuations are responsible for pattern formation in CO oxidation on macroscopic single crystal surfaces at high pressures [14]. At high pressure, the CO diffusion length will be reduced and, therefore, one can envision the catalytic surface as consisting of small homogeneous well-stirred regions coupled by CO diffusion. The number of particles inside each region is small and given that the amplitude of fluctuations in coverage scales inversely like the square root of the number of particles in the system, local coverage fluctuations become also important. Under these conditions, the interplay between a finite surface area and CO diffusion between confined surface regions start to play an important role.

To shed more light on the reaction behavior under those conditions, we focus in this section in a spatially extended model where a surface is divided into a square lattice of M subdomains denoted by i, which are supposed to be smaller than the diffusion length [12,13,24–26]. The surface area of each small subdomain is represented by A. For simplicity, we consider that the subdomains exhibit equal catalytic activity (e.g, identical sticking coefficients). The transition rates and population changes of the particle number of carbon monoxide ($N_{CO,i}$) and oxygen ($N_{O,i}$) caused by reactive events inside each subdomain are the same used in Section 2: $W_1^i(N_{CO,i}/N_{CO,i}+1)$, $W_2^i(N_{CO,i}/N_{CO,i}-1)$, $W_3^i(N_{O,i}/N_{O,i}+2)$, and $W_4^i(N_{CO,i}, N_{O,i}/N_{CO,i}-1, N_{O,i}-1)$. In this case, we also set $p_{O_2} = 0.25$ and $k = 100$. Before we start our analysis, we want to emphasize that inside each subdomain, bistability is observed for $d < d_C(A)$, where $d_C(A)$ corresponds to a cusp bifurcation point, see Fig. 1. Therefore, in order to prevent strong finite-size shifts described in Section 2, the partial pressure and desorption rates are chosen far away from the cusp point as $p_{CO} = 0.4168$ and $d = 0.4$, respectively. As an example, Fig. 4 shows the corresponding bimodal probability distribution for these parameter values.

CO(ads) hops to adjacent free sites of a nearest-neighbor subdomain at a rate h. The mass transport is thus mimicked by the displacement of CO(ads) from one subdomain to another at a rate given by $hN_{CO,i}/A$ times the probability that a site is empty in the other subdomains. We define the transition rates that describe this diffusion random walk as:

$$W_5^i(N_{CO,i}/N_{CO,i}-1) = \frac{h}{4A}N_{CO,i}\sum_l(1-\theta_{CO,i+l}-\theta_{O,i+l}), \tag{27}$$

$$W_6^i(N_{CO,i}/N_{CO,i}+1) = \frac{h}{4A}(1-\theta_{CO,i}-\theta_{O,i})\sum_l N_{CO,i+l}. \tag{28}$$

The sum l runs over the nearest neighbors of the cell i. $\theta_{CO,i}$ and $\theta_{O,i}$ are $N_{CO,i}/A$ and $N_{O,i}/A$, respectively. $W_5^i(N_{CO,i}/N_{CO,i}-1)$ represents the transition probability per unit time to decrease by diffusion the number of CO molecules from $N_{CO,i}$ to $N_{CO,i}-1$, and $W_6^i(N_{CO,i}/N_{CO,i}+1)$ represents the transition probability per unit time to increase by diffusion the number of CO molecules from $N_{CO,i}$ to $N_{CO,i}+1$. Adsorbed oxygen atoms are immobile and cannot desorb. The parameter h mimics the coupling intensity between the bistable subdomains.

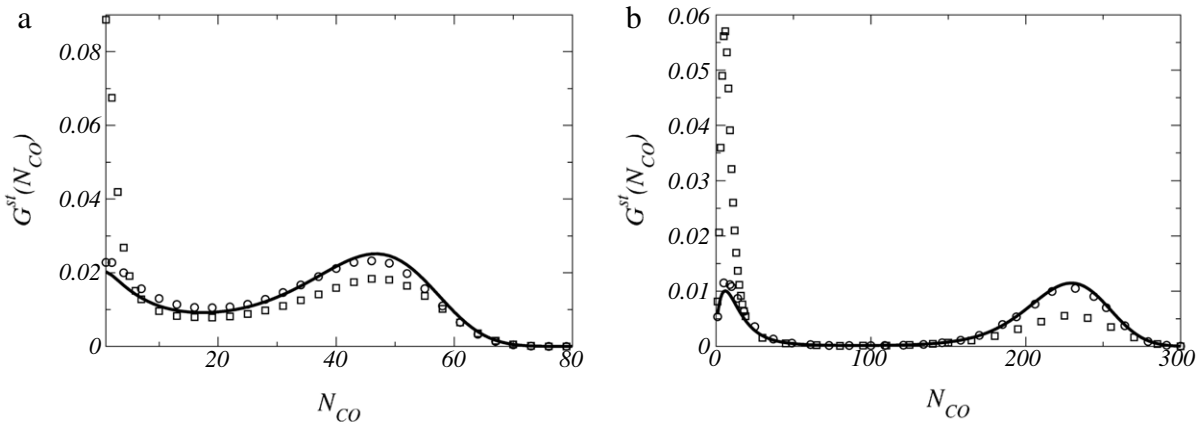

Fig. 4. Stationary probability distribution function $G^{\mathrm{st}}(N_{\mathrm{CO}})$ inside each subdomain obtained from theory (solid lines). The rates are $p_{\mathrm{CO}} = 0.4168$, $d = 0.4$, $p_{\mathrm{O}_2} = 0.25$, and $k = 100$. (a) $G^{\mathrm{st}}(N_{\mathrm{CO}})$ for $A = 100$. (b) $G^{\mathrm{st}}(N_{\mathrm{CO}})$ for $A = 500$. The theoretical results are compared with simulations using the direct Gillespie algorithm. Circles represent simulations from the adiabatically reduced model. Squares represent simulations from the original unreduced model. Note that if A increases, the transitions between the two stable states decreases.

The stochastic behavior of the system is described by the probability distribution function $P(\mathbf{Z}; t)$ of finding a set of populations $\mathbf{Z} = \{N_{\mathrm{CO},i}, N_{O,i}\}$, with $i = 1, \ldots, M$. It is well known that $P(\mathbf{Z}; t)$ is governed by the so-called reaction–diffusion master equation which results from the transition probabilities W_σ^i, where σ runs from 1 to 6. This equation can be expressed in a compact form as Ref. [27]

$$\frac{\mathrm{d}P(\mathbf{Z}; t)}{\mathrm{d}t} = \frac{\mathrm{d}P^{\mathrm{reac}}}{\mathrm{d}t} + \frac{\mathrm{d}P^{\mathrm{diff}}}{\mathrm{d}t}. \tag{29}$$

We have performed simulations of this equation using an extended version of Gillespie algorithm, which has been inspired by the next subvolume method introduced by Elf and Ehrenberg for simulating stochastic reaction–diffusion kinetics [17]. However, our main goal is to obtain analytical solutions.

3.1. Local description of fluctuations

The main feature of our approximation is to replace the local interaction between subdomains by an average interaction between one subdomain and the surrounding big system. In this way, the local character of fluctuations is preserved. We start by replacing the nearest-neighbor interaction by a global interaction through an average field or effective environment (Weiss mean-field approximation or all to all coupling). This means that $\frac{1}{4}\sum_l(1 - \theta_{\mathrm{CO},i+l} - \theta_{O,i+l})$ and $\frac{1}{4}\sum_l N_{\mathrm{CO},i+l}$ are replaced with $\frac{1}{M-1}\sum_{j=1,j\neq i}^{M}(1-\theta_{\mathrm{CO},j}-\theta_{O,j})$ and $\frac{1}{M-1}\sum_{j=1,j\neq i}^{M} N_{\mathrm{CO},j}$, respectively. Then, if the oxygen coverage is adiabatically eliminated from the master equation (29) as in Section 2 and the number of subdomains goes to infinity ($M \to \infty$), we find the following mean-field birth–death master equation of one small subdomain interacting with the surrounding big system [15]:

$$\begin{aligned}\frac{\mathrm{d}G(N_{\mathrm{CO}}, N_{\mathrm{CO}}^m; t)}{\mathrm{d}t} &= H_1(N_{\mathrm{CO}} - 1)G(N_{\mathrm{CO}} - 1, N_{\mathrm{CO}}^m; t) - H_1(N_{\mathrm{CO}})G(N_{\mathrm{CO}}, N_{\mathrm{CO}}^m; t)\\ &\quad + H_2(N_{\mathrm{CO}} + 1)G(N_{\mathrm{CO}} + 1, N_{\mathrm{CO}}^m; t) - H_2(N_{\mathrm{CO}})G(N_{\mathrm{CO}}, N_{\mathrm{CO}}^m; t),\end{aligned} \tag{30}$$

where the new transition probabilities are:

$$H_1(N_{\mathrm{CO}}/N_{\mathrm{CO}} + 1) = Ap_{\mathrm{CO}}\left[1 - \left(\frac{N_{\mathrm{CO}}}{A}\right)^2\right] + \frac{h(1 - \theta_{\mathrm{CO}} - \tilde{\theta}_{\mathrm{O}})N_{\mathrm{CO}}^m}{A}, \tag{31}$$

$$H_2(N_{\mathrm{CO}}/N_{\mathrm{CO}} - 1) = dN_{\mathrm{CO}} + \frac{4k\tilde{N}_{\mathrm{O}}N_{\mathrm{CO}}}{A} + \frac{hN_{\mathrm{CO}}(1 - \theta_{\mathrm{CO}}^m - \tilde{\theta}_{\mathrm{O}}^m)}{A}. \tag{32}$$

The fluctuation in the number of particles is controlled by the surface area A, which satisfies $0 < N_{\mathrm{CO}} + N_{\mathrm{O}} \leq A$. $\tilde{N}_{\mathrm{O}}$ and $\tilde{N}_{\mathrm{O}}^m$ emphasize that oxygen has been adiabatically eliminated. Here, we also suppose that the time-scale separation between the two random variables N_{O} and N_{CO} is large enough, and that the fast variable $\tilde{N}_{\mathrm{O}} = A\tilde{\theta}_{\mathrm{O}}$ can be approximated using the corresponding deterministic equation (12) with θ_{CO} being kept constant.

Now, it is possible to introduce the order parameter or self-consistent equation

$$N_{\mathrm{CO}}^m = \beta(N_{\mathrm{CO}}^m) = \sum_{N_{\mathrm{CO}}} N_{\mathrm{CO}}G^{\mathrm{st}}(N_{\mathrm{CO}}, N_{\mathrm{CO}}^m), \tag{33}$$

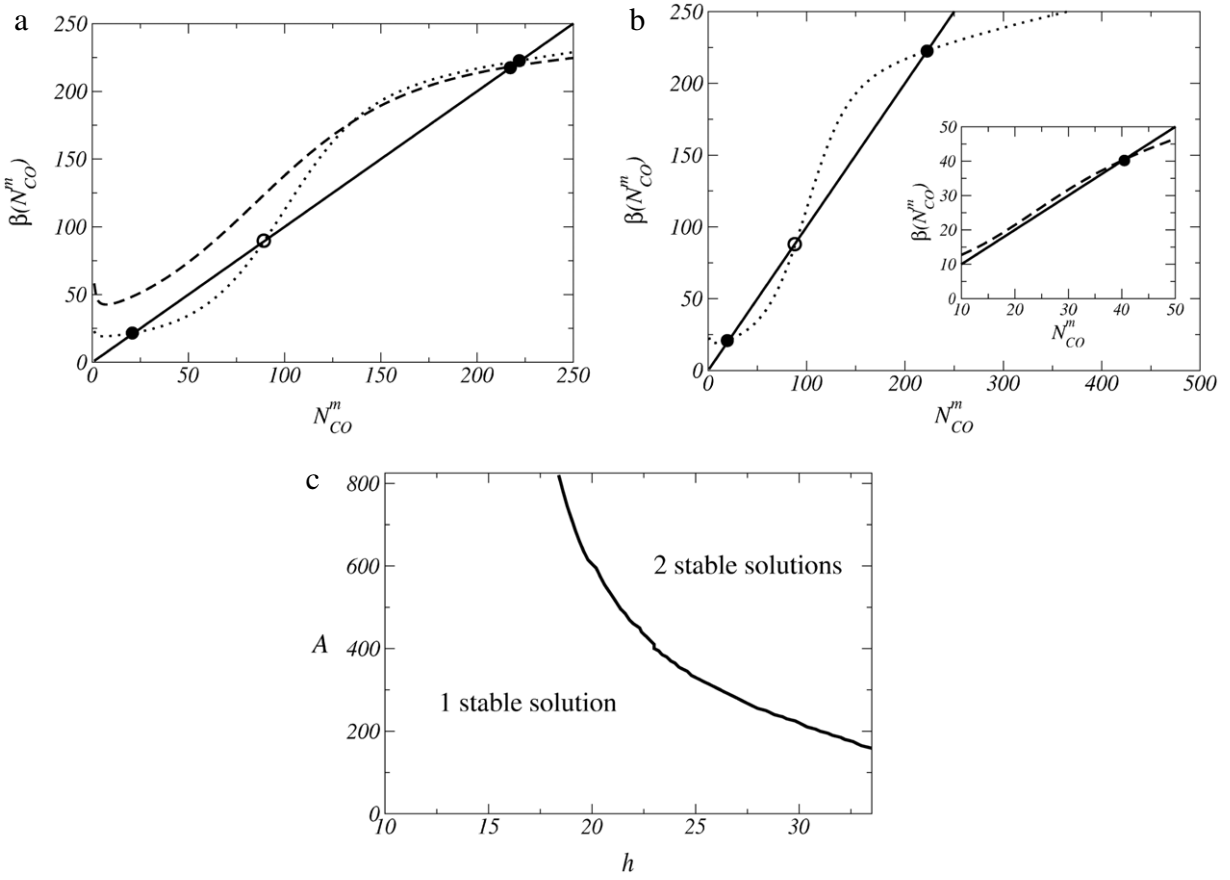

Fig. 5. Solutions of the self-consistent Eq. (33) and the corresponding phase diagram for $p_{CO} = 0.4168$, $d = 0.4$, $p_{O_2} = 0.25$, and $k = 100$. The solutions are given by the intersection of $\beta(N^m_{CO})$ with the diagonal line. (a) Solutions for $A = 500$ with $h = 15$ (dashed line) and $h = 30$ (dotted line). The two extreme solutions are stable (solid dots) and the intermediate one unstable (open dot). Note the transition from one to two stable solutions indicating a first-order phase transition. (b) As for (a) but for $h = 30$ and two values of A. Inset shows the case $A = 100$ (dashed line) and the main figure shows the case $A = 500$ (dotted line). The phase transition as a function of A is also evident. (c) Phase diagram on the parameter space (A, h).

which is a nonlinear equation for the unknown value N^m_{CO}. The multiple solutions of this equation reflect the possibility of bifurcations that break the ergodicity associated with the presence of a true phase transition. This simplification allows us to introduce an effective potential for each subdomain

$$\phi(N_{CO}, N^m_{CO}) = \frac{-\ln G^{st}(N_{CO}, N^m_{CO})}{A}, \tag{34}$$

where the new probability distribution function of one subdomain and its very large environment can also be written, after invoking the detailed balance, as

$$G^{st}(N_{CO}, N^m_{CO}) = \prod_{N=1}^{N_{CO}} \frac{H_1(N-1)}{H_2(N)} \left(1 + \sum_{n=1}^{A} \prod_{N=1}^{n} \frac{H_1(N-1)}{H_2(N)}\right)^{-1}. \tag{35}$$

Note that the order parameter is the mean value of CO coverage obtained from $G^{st}(N_{CO}, N^m_{CO})$. In our problem, two cases are possible. (i) The probability distribution is unique, and the order parameter has only one solution. (ii) We have several probability distributions, and the order parameter has several solutions, one for each probability distribution.

We proceed to plot in Fig. 5 the typical behavior of Eq. (33). Fig. 5(a) shows the onset of the stable solutions of the self-consistency condition as a function of h with A fixed. Fig. 5(b) shows also the onset of several solutions but now as a function of A with h fixed. The two extreme solutions are stable (solid dots) and the intermediate one unstable (open dot). In Fig. 5(c), we construct the corresponding phase diagram in the parameter space (A, h). This diagram is divided into two regions according to the behavior mentioned above. It is evident that our theory predicts a first-order phase transition in our globally coupled system with infinite number of subdomains as a function of the surface area A and coupling parameter h.

In order to analyze the bifurcation behavior as a function of surface area A, we compare the results obtained by solution of the self-consistency condition with stochastic simulations of the original unreduced model for a finite number of

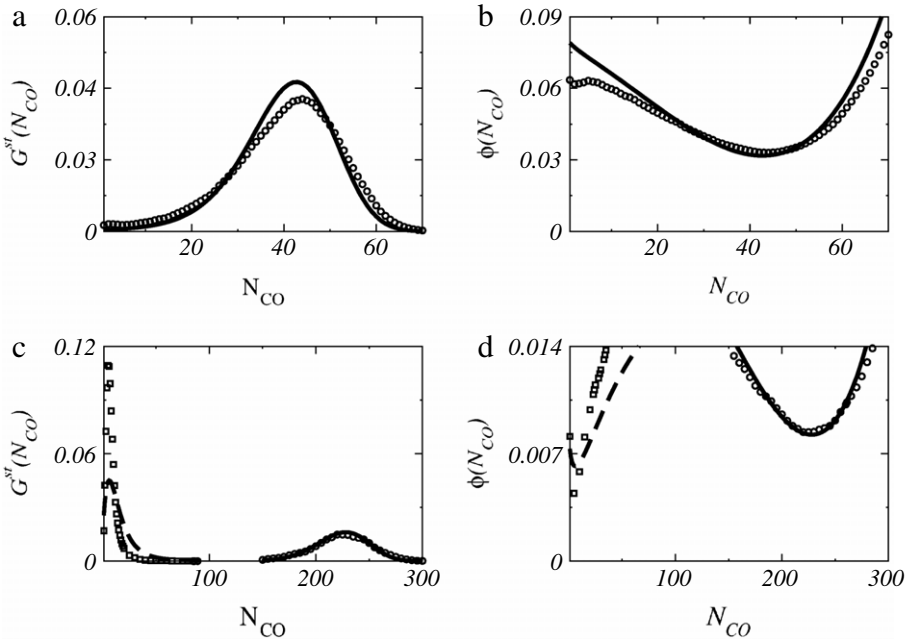

Fig. 6. Probability distributions and effective potentials from theory and stochastic simulations of a globally coupled system with 32 subdomains as a function of the surface area A. Top panels show $G^{st}(N_{CO})$ and $\phi(N_{CO})$ for $A = 100$. Bottom panels show $G^{st}(N_{CO})$ and $\phi(N_{CO})$ for $A = 500$. The coupling parameter is fixed as $h = 30$. Subdomain parameters are $p_{CO} = 0.4168$, $d = 0.4$, $p_{O_2} = 0.25$, and $k = 100$. Dashed and solid lines are theoretical results. The numerical analysis is performed by sampling trajectories over a time scale during which no jumps between the components from theory occur (symbols). Simulations start with same number of CO molecules for each subdomain. We have fixed those initial conditions always around the maxima of the probability distribution functions predicted by the theory. Histograms are obtained at arbitrary subdomain i.

subdomains. We will show that although for finite systems there is not perfect separation into the components from the ergodicity breaking theory, the histograms obtained from simulations follow very closely the probability distributions of these components. The analysis is performed by sampling trajectories over a time scale during which the solutions from the ergodicity breaking theory establishes and no jumps between these solutions occur.

We start showing simulations of a globally coupled system. We have implemented the Gillespie algorithm to include all to all coupling between subdomains. The main idea is to suppose that each subdomain interacts with a very large effective environment composed by the rest of subdomains. In Fig. 6, we compare $G^{st}(N_{CO})$ and $\phi(N_{CO})$ from theory with stochastic simulations using 32 subdomains. We have fixed $h = 30$ and plotted the behavior as a function of A. Simulations start with the same number of CO molecules for each subdomain. These initial conditions are fixed always around the maxima of the probability distributions predicted by theory. Histograms are obtained for one arbitrary chosen subdomain. Fig. 6(a) and (b) show the case $A = 100$. Here, the theory predicts only one maxima for $G^{st}(N_{CO})$ or minima for $\phi(N_{CO})$. Simulations very well reproduce the analytical results (circles). However, if one increases A the theory predict a perfect separation into different components or monomodal probability distributions indicating a first-order phase transition. This result is plotted in Fig. 6(c) and (d), where two components are shown. They represent states of low (dashed lines) and high (solid lines) number of CO molecules inside each subdomain. Stochastic simulations very well confirm this behavior (squares and circles). The main discrepancy comes from imposed approximations. Note that the initial conditions determine which of the components is selected.

The stochastic simulations on a square lattices exhibit a similar qualitative behavior, but the quantitative agreement with theory is, as expected, less satisfactory. Fig. 7 is similar to Fig. 6, but in this case we compare $G^{st}(N_{CO})$ and $\phi(N_{CO})$ from the theory with stochastic simulations on a square lattice with nearest-neighbor coupling. We consider for simulations 32×32 subdomains and periodic boundary conditions. Although for our finite system there is not perfect separation into different components, the trajectories follow very closely the probability distributions of the components predicted by theory.

We emphasize that, because the number of subdomains M as well as the surface are A are small, fluctuation-induced transition between the different components from the theory would occur after long simulation time. Therefore, the obtained histograms are true on a time scale after which the two solutions practically establishes. But there is a long- time scale where ergodicity is reached. At this large time scale, we find transitions between the two stable components which become more frequent with decreasing the number of subdomains; cf. Fig. 8. The smaller M, the shorter the transition times between components from the ergodicity breaking theory.

4. Summary and conclusions

In this article, we investigate analytically the impact of surface size on minimalistic models for the bistable CO oxidation. Motivated by recent experiments of CO oxidation on nanoscale surfaces, we introduce a stochastic mean-field model and

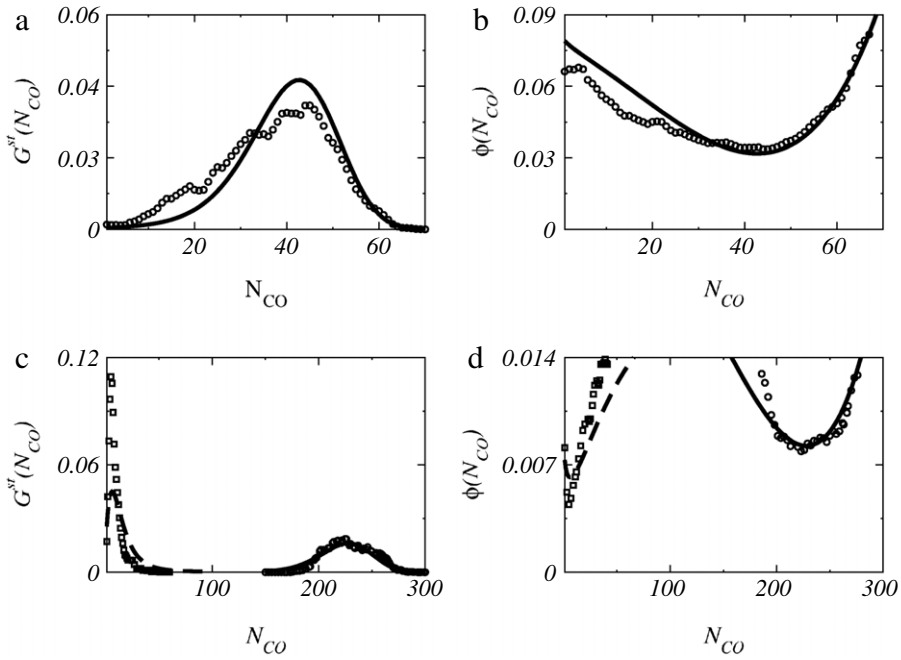

Fig. 7. Similar to Fig. 6, but with the probability distribution and effective potential obtained from stochastic simulations on a square lattice of 32 × 32 subdomains with nearest-neighbor coupling and periodic boundary conditions (symbols).

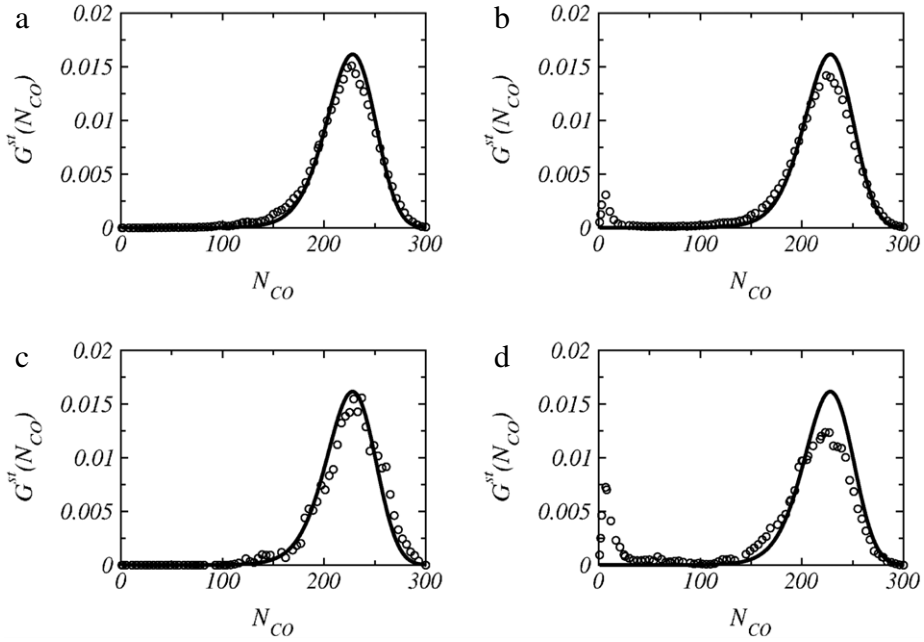

Fig. 8. Top panels show the time development of the probability distribution function for a globally coupled system with 10 subdomains (circles). Bottom panels show the time development of the probability distribution function for a locally coupled system with 16 × 16 subdomains (circles). For the case of global coupling, the simulation times are (a) $t = 5167.26$ and (b) $t = 15\,349.52$. For the case of local coupling, the simulation times are (c) $t = 198.58$ and (d) $t = 670.55$. The coupling parameter is fixed as $h = 30$. Subdomain parameters are $A = 500$, $p_{CO} = 0.4168$, $d = 0.4$, $p_{O_2} = 0.25$, and $k = 100$. Solid lines are theoretical results. We have fixed the initial conditions always around the maxima of the theoretical probability distribution functions represented by these solid lines. Histograms are obtained at arbitrary subdomain i. Note that after a certain transient time a maxima starts to form around the second stable component predicted by the theory. This indicates that for finite systems the ergodicity is reached after a certain simulation time.

show analytically and by simulations that a shift of the bistable region occurs when we decrease or increase the surface area. Analytical results are obtained after the adiabatic elimination of the fast oxygen coverage from the mean-field master

equation. We derive the stationary probability distribution and introduce an effective potential that can be used to quantify coverage fluctuations.

We introduced a compartmentalized model suitable to study CO oxidation under reduced diffusion length of CO particles. We have studied local fluctuations by invoking the Weiss mean-field approximation together with the adiabatic elimination of oxygen variable. In the Weiss mean-field approximation, we replace the nearest-neighbor interaction by an all to all coupled system of infinitely many bistable constituents. This allows an analytical estimation of the probability distribution function and effective potential. The theory provides evidence for an ergodicity breaking associated with a first-order phase transition as a function of the size of the surfaces. In order to verify our results, the Gillespie algorithm was implemented to include global as well as nearest-neighbor coupling. Histograms, obtained by sampling trajectories over a time during which no jumps between the components from the ergodicity breaking theory occur, following very closely the probability distribution of the components predicted by theory.

The shift of the bistable regions is a genuine finite-size effect that should be observed in experiments. We recall that size effects have been already observed in CO oxidation on a Pt field emitter tip [3,5,4]. Interestingly, it has been reported that the smaller the (112) facets the farther away from the critical point of the kinetic phase diagram the fluctuation-induced transitions occur [4]. We also expect that the coupling between different facets will lead to additional finite-size effects.

Further work will address the impact that the interplay between coverage and parametric fluctuations has on surface reactions [28,29]. An interesting extension could be to use stochastic models, like the master equations used in this work, in order to study an array of nanoparticles coupled globally through the gas phase [30] or an ensemble of electrochemical nano-oscillators [31]. Our spatially extended stochastic model can in principle be used to study fluctuations on inhomogeneous metal surfaces, where structural defects such steps or impurities are present. The structural defects can be considered as small regions on the surface with different kinetic parameters coupled by CO diffusion.

Acknowledgements

M.P acknowledges the financial support of project FIS2007-60327 from MICINN (Spain) and FEDER (EU). LSG acknowledges support by DFG through Sfb555.

References

[1] N. Pavlenko, J.W. Evans, D.J. Liu, R. Imbihl, Phys. Rev. E 65 (2001) 016121.
[2] J.S. McEwen, P. Gaspard, T.V. de Bocarmé, N. Kruse, Proc. Natl. Acad. Sci. USA 106 (2009) 3006.
[3] Y. Suchorski, J. Beben, E.W. James, J.W. Evans, R. Imbihl, Phys. Rev. Lett. 82 (1999) 1907.
[4] Y. Suchorski, J. Beben, R. Imbihl, E.W. James, D.J. Liu, J.W. Evans, Phys. Rev. B 63 (2001) 165417.
[5] Y. Suchorski, J. Beben, R. Imbihl, Prog. Surf. Sci. 59 (1998) 343.
[6] V. Johánek, M. Laurin, A.W. Grant, B. Kasemo, C.R. Henry, J. Libuda, Science 304 (2004) 1639.
[7] D.J. Liu, J.W. Evans, J. Chem. Phys. 117 (2002) 7319.
[8] M. Pineda, R. Imbihl, L. Schimansky-Geier, Ch. Zülicke, J. Chem. Phys. 124 (2006) 044701.
[9] N. Pavlenko, R. Imbihl, J.W. Evans, D.J. Liu, Phys. Rev. E 68 (2003) 016212.
[10] Y. Gong, Z. Hou, H. Xin, J. Phys. Chem. B 108 (2004) 17796.
[11] Y. Gong, Z. Hou, H. Xin, J. Phys. Chem. A 109 (2005) 2741.
[12] F. Chávez, R. Kapral, Phys. Rev. E 63 (2000) 016211.
[13] H. Wang, Z. Fu, X. Xu, Q. Ouyang, J. Phys. Chem. A 111 (2007) 1265.
[14] J. Starke, C. Reichert, M. Eiswirth, H.H. Rotermund, G. Ertl, Europhys. Lett. 73 (2006) 820.
[15] M. Pineda, L. Schimansky-Geier, R. Imbihl, Phys. Rev. E 75 (2007) 061107.
[16] D.T. Gillespie, J. Chem. Phys. 122 (1977) 2340.
[17] J. Elf, M. Ehrenberg, Systems Biol. 1 (2004) 230.
[18] R. Imbihl, G. Ertl, Chem. Rev. (Washington, DC) 95 (1995) 697.
[19] C. Reichert, J. Starke, M. Eiswirth, J. Chem. Phys. 115 (2001) 4829.
[20] C.V. Rao, A.P. Arkin, J. Chem. Phys. 118 (2003) 4999.
[21] M. Bär, Ch. Zülicke, M. Eiswirth, G. Ertl, J. Chem. Phys. 96 (1992) 8595.
[22] Y. Cao, D.T. Gillespie, L.R. Petzold, J. Chem. Phys. 81 (2005) 014116.
[23] W. Ebeling, L. Schimansky-Geier, Physica A 98 (1979) 587.
[24] A. Chatterjee, D.G. Vlachos, J. Chem. Phys. 124 (2006) 064110.
[25] S. Lampoudi, D.T. Gillespie, L.R. Petzold, J. Chem. Phys. 130 (2009) 094104.
[26] D. Bernstein, Phys. Rev. E 71 (2005) 041103.
[27] C.W. Gardiner, Handbook of Stochastic Methods for Physics, Chemistry and the Natural Science, Springer-Verlag, Berlin, 1985.
[28] S. Wehner, P. Hoffmann, S. Schmeisser, H.R. Brand, J. Küppers, Phys. Rev. Lett. 95 (2005) 1907.
[29] M. Pineda, R. Toral, J. Chem. Phys. 130 (2009) 124704.
[30] N.V. Peskov, M.M. Slinko, N.I. Jaeger, J. Chem. Phys. 118 (2003) 8882.
[31] I.Z. Kiss, W. Wang, J.L. Hudson, J. Phys. Chem. B 103 (1999) 11433.